Title

Constraining the Halo Mass of Damped Lyα Absorption Systems (DLAs) at z = 2—3.5 Using the Quasar–CMB Lensing Cross-correlation

Authors

Lin, Xiaojing
Cai, Zheng
Li, Yin
et al.

Peer reviewed

Constraining the Halo Mass of Damped Lyα Absorption Systems (DLAs) at $z = 2 - 3.5$ using the Quasar-CMB Lensing Cross-correlation

Xiaojing Lin,[1] Zheng Cai,[2] Yin Li,[3] Alex Krolewski,[4,5] and Simone Ferraro[5]

[1]*Department of Astronomy, School of Physics, Peking University, Beijing 100871, China*
[2]*Department of Astronomy, Tsinghua University, Beijing 100084, China*
[3]*Center for Computational Astrophysics & Center for Computational Mathematics, Flatiron Institute, 162 5th Avenue, 10010, New York, NY, USA*
[4]*Department of Astronomy, University of California, Berkeley, CA 94720*
[5]*Physics Division, Lawrence Berkeley National Laboratory, Berkeley, CA*

ABSTRACT

We study the cross correlation of damped Lyα systems (DLAs) and their background quasars, using the most updated DLA catalog and the *Planck* 2018 CMB lensing convergence field. Our measurement suggests that the DLA bias $b_{\rm DLA}$ is smaller than 3.1, corresponding to $\log(M/M_\odot h^{-1}) \leq 12.3$ at a confidence of 90%. These constraints are broadly consistent with Alonso et al. (2018) and previous measurements by cross-correlation between DLAs and the Lyα forest (e.g. Font-Ribera et al. 2012; Pérez-Ràfols et al. 2018). Further, our results demonstrate the potential of obtaining a more precise measurement of the halo mass of high-redshift sources using next generation CMB experiments with a higher angular resolution. The python-based codes and data products of our analysis are available at https://github.com/LittleLin1999/CMB-lensingxDLA.

Keywords: CMB, weak lensing — large-scale structure — quasar, DLA — halo mass

1. INTRODUCTION

Damped Lyα systems (DLAs) are a class of absorbers along the QSO sight lines with high neutral hydrogen (HI) column densities of $N_{\rm HI} \geq 2 \times 10^{20}$ cm^{-2} (Wolfe et al. 1986). They are featured by their damping wings absorption profile, a result of the quantum natural broadening of the HI Lyα transition. DLAs are thought to dominate the neutral-gas content of the Universe in the redshift range of $0 \leq z \leq 5$ (Wolfe et al. 2005), acting as important neutral gas reservoirs for star formation (e.g. Nagamine et al. 2004; Ota et al. 2014; Rudie et al. 2017). They can also be a powerful cosmological probe for related research, such as studying the hosts of quasars (e.g. Hennawi et al. 2009; Zafar et al. 2011; Cai et al. 2014).

Over the last three decades, a number of attempts have been made to discover the nature of DLAs by directly probing the emission of the DLA galaxies using the largest optical or infrared telescopes (e.g. Le Brun et al. 1997; Møller et al. 2002; Chen et al. 2005). These studies have been moderately successful at low redshift. Nevertheless, after the many deep observations with innovative techniques (e.g. Kulkarni et al. 2006; Fynbo et al. 2010; Fumagalli et al. 2015; Johnson-Groh et al. 2016), only about 20 DLA host galaxies at $z \gtrsim 2$ have been identified. These results suggest that DLA host galaxies have a relatively small, sub-L^* galaxies with the star formation rate (SFR) of $\sim 0.1 - 10$ $M_\odot$ yr^{-1} (e.g., Krogager et al. 2017). With the Atacama Large Millimeter/submillimeter Array (ALMA), Neeleman et al. (2018, 2020) have revealed a small sample (< 10) of host galaxies of high-metallicity DLAs at $z \approx 4$ using the sub-millimeter observations. They find that the SFR of DLA hosts is on the order of 10 - 100 $M_\odot$ yr^{-1}, indicating that metal-rich DLA hosts could be super-L^* galaxies, at odds with the previous findings.

linxiaojing@pku.edu.cn

zcai@mail.tsinghua.edu.cn

yinli@flatironinstitute.org

Statistical studies of the DLA hosts also remain unclear and controversial. Several works measure the DLA bias by studying the cross-correlation between DLAs and other tracers, such as Lyman break galaxies (e.g. Cooke et al. 2006; Lee et al. 2011) and Lyα forests (e.g. Font-Ribera et al. 2012; Pérez-Ràfols et al. 2018). The latter imply that DLAs are hosted by massive halos with typical masses of $10^{11} - 10^{12} M_\odot$. Mass-metallicity statistics reveal that the DLA hosts should have a stellar mass of $10^{8.5}$ $M_\odot$ (e.g. Møller et al. 2013). This result is also supported by several hydrodynamical simulations (e.g. Pontzen et al. 2008; Berry et al. 2016) which suggest that DLA galaxies have stellar masses ranging from 10^6 $M_\odot$ to 10^{11} $M_\odot$, with the median value around 10^8 $M_\odot$. More statistical efforts are needed to provide more independent measurements on the DLA hosts.

Besides the detection techniques mentioned above, weak lensing of the cosmic microwave background (CMB) is a powerful tool to probe halo mass at high redshift. The cross-correlation between the CMB and other tracers of large-scale structure can be used to measure the tracer bias , with which one can infer the typical halo masses of the tracer populations. The cross-correlation measurement is not prone to systematic effects that are possibly present in the auto-correlation approach, such as incompleteness, random catalog generation, masking, etc.(Reid et al. 2016; Geach et al. 2019). This technique has been performed to analyse the clustering properties of quasars and galaxies and provide strong cosmological constraints (e.g. Sherwin et al. 2012; Bianchini et al. 2015; Krolewski et al. 2019). Likewise, CMB photons are deflected not only by the quasar hosts, but also by DLAs in the sightlines. The measured gravitational magnification of the background quasars would be strongly affected by the foreground DLAs if DLAs reside in massive halos comparable to those of the quasar hosts. The assumption has been confirmed by studies on the CMB lensing-quasar cross-correlations using quasars with and without DLAs in their sightlines (Alonso et al. 2018).

In this paper we carefully measure the cross-correlation between the *Planck* CMB lensing convergence map and two quasar overdensity maps. One of the two quasar maps ensures that each quasar sight line contains at least one DLA. Through comparing the cross-correlation results of the two maps, the properties of DLA host are extracted. In § 2 we introduce the data samples used in this work. § 3 presents the estimator of the cross-correlation power spectrum and its error. In § 4 we measure the biases of the quasar and DLA samples. The null test results are reported in § 5. In § 6 we discuss our measurements and their consistency with several previous works. We draw our conclusions in § 7. Additionally, we apply simple tests by applying this approach to a quasar bias evolution model, a tSZ-free CMB lensing map and another DLA catalog in Appendix A, B, and C. Throughout the paper, we adopt a flat Λ cold dark matter (ΛCDM) cosmological model as described in Planck Collaboration et al. (2018a), with H_0=67.4, Ω_m=0.315, $\Omega_b h^2$=0.0224, $\Omega_c h^2 = 0.120$.

2. DATA SAMPLE

2.1. *BOSS quasars*

Both of our QSOs and DLAs are selected from the third stage of the SDSS survey (SDSS III, Eisenstein et al. 2011). SDSS-III mapped a total of 14,555 unique square degrees of the sky, including contiguous areas of $\sim 7,500$ deg^2 in the North Galactic Cap (NGC) and $\sim 3,100$ deg^2 in the South Galactic Cap (SGC) using the Sloan Foundation 2.5-meter Telescope at Apache Point Observatory in New Mexico. As the main dark time survey of SDSS III, the Baryon Oscillation Spectroscopic Survey (BOSS) (BOSS, Dawson et al. 2013) observed about 300,000 quasars, and 184,000 of which fall within the redshift range of $2.15 \leq z \leq 4$. BOSS detected the baryon acoustic oscillation (BAO) using HI absorption lines in the intergalactic medium (IGM) at z∼2.5 (Busca et al. 2013). The quasar samples used in our work are from the final SDSS-III/BOSS quasar catalog[1] (Pâris et al. 2017), containing 184,101 quasars at $z \geq 2.15$, with 167,742 of them being new discoveries.

2.2. *Planck 2018 data*

The Planck satellite, launched on 14 May 2009, mapped the anisotropies of the cosmic microwave background (CMB) at multiple frequencies with a high sensitivity and small angular resolution. *Planck* 2018 results (Planck Collaboration et al. 2018b) provide variations of lensing potential estimates as tables of spherical harmonic coefficients up to $\ell = 4096$, as well as a lens reconstruction analysis mask in the HEALPix format (Górski et al. 2005) with $N_{side} = 2048$, i.e. a pixel side of $d_{pix} \approx 1.7$ arcmin. The lensing convergence map[2] we use was reconstructed by the minimum-variance (MV) estimate (Carron & Lewis 2017) from temperature and polarization, covering approximately 70% of the sky.

---

[1] https://www.sdss.org/dr12/algorithms/boss-dr12-quasar-catalog/

[2] Lensing products are are available from the Planck Legacy Archive: https://pla.esac.esa.int/#cosmology

2.3. *DLA catalog*

We utilize a DLA catalog classified by a convolutional neural network (CNN) based DLA finder (Parks et al. 2018). The CNN architecture used multi-task learning to characterize strong HI Lyα absorption in quasar spectra, and estimated the corresponding redshift z_{abs} and HI column density N_{HI}. By comparing the absorption redshifts and N_{HI} values between the matched DLAs from their algorithm and that in Garnett et al. (2017a), they measured small mean offsets of $\Delta z = -0.00035$ and $\Delta N_{HI} = -0.038$ and standard deviations of 0.002 and 0.16 dex respectively. The model also outputs a *confidence* parameter to depict the confidence level based on how precisely the CNN model predicted the location of the DLA. The model classified and measured absorption lines of DLAs in sightlines in the SDSS-III/DR12 QSO database (Pâris et al. 2017). The resulted catalog has 50,969 systems with $\log N_{HI} \geq 20.3$, $z_{abs} > 2$, and $z_{abs} < z_{em}$, in the 174,691 sightlines not flagged as broad absorption lines (BALs) in the BOSS quasar catalog.

As a test we also apply our analysis to the DLA catalog released by Ho et al. (2020). More details are present in Appendix C.

2.4. *Sample selection*

We apply a series of constraints on the BOSS catalog similar to that in Eftekharzadeh et al. (2015). One of our selection criteria is to reject quasars that are detected at 1.4 GHz by the Faint Images of the Radio Sky at Twenty-Centimeters (FIRST) survey (Becker et al. 1995). Radio-loud quasars are removed because they may cluster differently from optically selected quasars(Donoso et al. 2010; Retana-Montenegro & Röttgering 2017). Our selection criteria are the follows:

- *1st cut*: we include only quasars in the redshift range of $2.2 < z < 3.4$.
- *2nd cut*: a magnitude cut of $m_g < 22$ is applied.
- *3rd cut*: a luminosity cut of $-28.74 < M_i < -23.78$ is applied. M_i refers to the absolute i-band magnitude K-corrected to $z = 2$, and has been calculated for each quasar by SDSS(Richards et al. 2006).
- *4th cut*: we limit our measurements to the NGC region, because some previous analyses (e.g. White et al. 2012; Eftekharzadeh et al. 2015) have reported unexplained differences between clustering measurements in the BOSS NGC and SGC regions.
- *5th cut*: quasars detected by the FIRST survey are excluded.

For DLA samples, we additionally eliminate broad absorption line (BAL) systems, whose profiles can be easily confused with the Voigt profiles of DLAs, and apply a confidence cut of *confidence* ≥ 0.3 (Parks et al. 2018), besides the constraints above. The total sample size of the subset of BOSS quasars is 105,642. And the final DLA catalog includes 17,774 quasars with 20,848 DLAs in their sightlines.
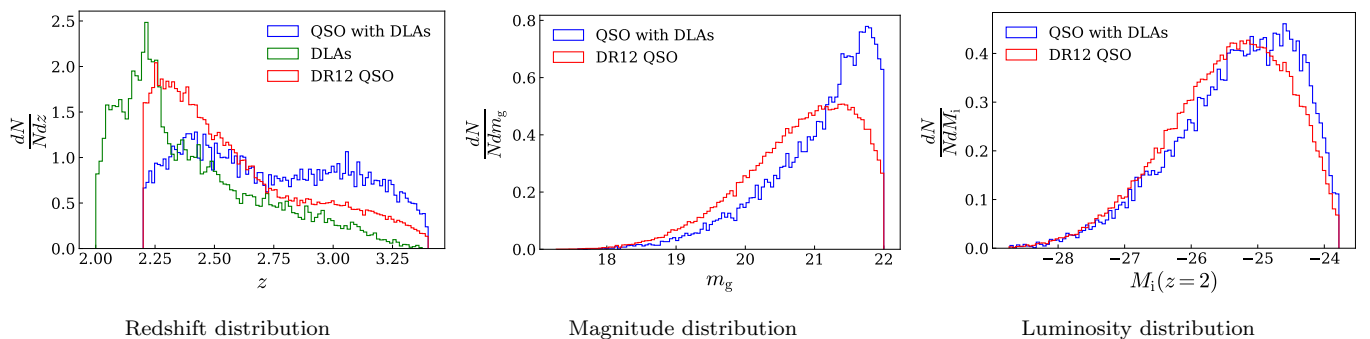

Redshift distribution · Magnitude distribution · Luminosity distribution

Figure 1. The normalised redshift, magnitude and luminosity distributions of our selected BOSS quasar and DLA samples.

3. METHODOLOGY

3.1. *Map construction and mask apodization*

To match the resolution of the CMB lensing convergence map, we construct the quasar overdensity maps in the HEALPix format (Górski et al. 2005) with $N_{\rm side} = 2048$, corresponding to 50,331,648 pixels for the whole sky:

$$q_i = \frac{n_i - \bar{n}}{\bar{n}} \tag{1}$$

where i is the pixel number, q_i is the quasar overdensity in the i-th pixel, and n_i is the quasar number counts in each pixel with $\bar{n}$ being its mean value.

Mask apodization is commonly used in the cross-correlation calculation to avoid Gibbs-ringing induced by a sharp cut-off in a map during the harmonic transformation. We give the brief procedures on mask construction and apodization below, and visualize the apodized mask in Fig. 2.

(i) We adopt the CMB lensing mask released by the Planck Collaboration as part of the *Planck* 2018 CMB lensing products. As for the BOSS quasar masks, we lower the resolution of the quasar overdensity maps to $N_{\rm side} = 32$ to identify the region covered by the SDSS survey. $N_{\rm side} = 32$ corresponds to 12,288 pixels or an angular resolution of 109.9 arcmin. This relatively low resolution is also chosen by Han et al. (2019) and Vielva & Sanz (2010), to represent a continuous sky coverage allowed by the survey. We label the empty pixels 0 and the remaining 1 to construct the quasar mask. A more accurate mask could be obtained from the random catalogs. We tried to use the CMASS random catalog provided by BOSS and get $f_{\rm sky}^{\kappa q} = 0.184$ (the fraction of the sky shared by the quasar overdensity map and the CMB lensing convergence map. See Eq.2 for more details), very close to the original $f_{\rm sky}^{\kappa q} = 0.179$ by downgrading the quasar map, making negligible difference to the final results.

(ii) These masks are upgraded to $N_{\rm side} = 2048$ again before performing the cross-correlation, to match the resolution of quasar maps and the CMB lensing map.

(iii) We apodize the masks by smoothing both the CMB mask and the quasar mask using a Gaussian kernel. To decide a proper kernel size, we generate 200 mocks based on a theoretical template, and apply masks smoothed by Gaussian kernels with FWHM of 10 arcmin, 30 arcmin and 1 degree, as well as a mask without smoothing. Then we calculate the mean squared error (MSE) of the residuals. A more detailed description for this procedure is given in Appendix D. We find that the mask smoothed by a Gaussian kernel with FWHM of 10 arcmin produces the minimal residual and thus should be the optimal choice.

FWHM	no smoothing	10 arcmin	30 arcmin	1 deg
MSE/$\times 10^{-19}$	2.33	2.08	3.63	8.21

Table 1. Comparison of different smoothing kernels, of width FWHM. MSE denotes the deviation of average binned spectra of the 200 Gaussian mocks from the theoretical template.
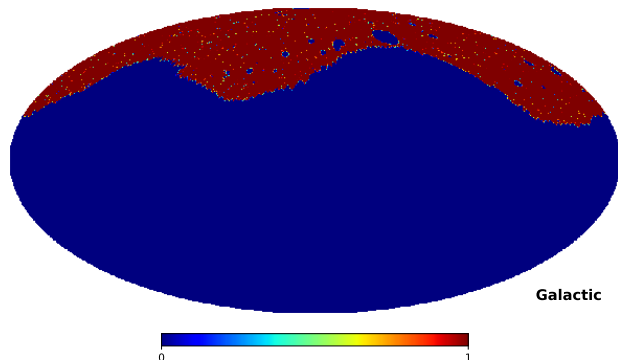

Figure 2. Apodized mask used to cross-correlated the quasar fields and CMB lensing convergence field. The mask has been smoothed by a Gaussian kernel of FWHM of 10 arcmin.

3.2. *Angular cross-power spectrum estimator*

We compute the CMB lensing-quasar overdensity angular cross-power spectrum using a pseudo-C_ℓ estimator (Wandelt et al. 2001a):

$$\hat{C}_\ell^{\kappa q} = \frac{1}{f_{\mathrm{sky}}^{\kappa q}} \sum_{m=-\ell}^{\ell} \kappa_{\ell m}^* q_{\ell m} \tag{2}$$

where $f_{\mathrm{sky}}^{\kappa q}$ is the fraction of the sky shared by the quasar overdensity map and the CMB lensing convergence map. $\kappa_{\ell m}$ and $q_{\ell m}$ are the spherical harmonic transforms of the CMB lensing convergence and the quasar overdensity maps, respectively. Note the $1/f_{\mathrm{sky}}^{\kappa q}$ estimator is known to be slightly biased (Wandelt et al. 2001b). However, while approximate, this should be good enough for our setup due to the noise level of the spectra. The transform can be computed readily by the anafast function within healpy[3]. We bin both the BOSS QSO and QSO with DLAs cross-power spectra into 10 bands over the range of $100 < \ell < 1200$. We apply a low-ℓ scale cut with $\ell_{\mathrm{min}} = 100$ because the cross correlation on $\ell < 100$ is deficient due to potential systematics shared by the quasar overdensity map and the CMB lensing map. This deficit of power at $\ell < 100$ is also found in Han et al. (2019); Pullen et al. (2016); Ferraro et al. (2016), for which we have not found compelling explanations. Some large scale systematics tracing the quasars may account for this (e.g. Geach et al. 2019).

Although Planck Collaboration et al. (2018b) has restricted the lensing auto-spectrum to the range of $8 \le \ell \le 400$ in the likelihood, ensuring robustness of the reconstruction only over this range, we perform a measurement on a higher multipole range with $\ell_{\mathrm{max}} = 1200$ [4], expecting both noise and systematics to be subdominant over this range as discussed in Giannantonio et al. (2016).

3.3. Cross-power spectrum covariance matrix

There are two common ways to estimate the statistical errors on the cross-power spectrum. One is through analytical calculation assuming both fields are Gaussian (Cabré et al. 2007; Hivon et al. 2002; Efstathiou 2004):

$$\frac{1}{\sigma_i^2(A)} = \sum_{l_{\mathrm{min}}(A) < l < l_{\mathrm{max}}(A)} \frac{f_{\mathrm{sky}}^{\kappa q}(2l+1)}{\left(C_l^{\kappa q}\right)^2 + C_l^{\kappa\kappa} C_l^{qq}} \tag{3}$$

where σ_i^2 is the error of the cross power in the i-th bin. $C_\ell^{\kappa\kappa}$ and C_ℓ^{qq} are the expected CMB lensing and quasar auto-power spectra, including both signal and noise. The estimators of the auto-power spectra are

$$\hat{C}_\ell^{\kappa\kappa} = \frac{1}{f_{\mathrm{sky}}^{\kappa}(2\ell+1)} \sum_{m=-\ell}^{\ell} |\kappa_{\ell m}|^2, \tag{4}$$

$$\hat{C}_\ell^{qq} = \frac{1}{f_{\mathrm{sky}}^{q}(2\ell+1)} \sum_{m=-\ell}^{l} |q_{\ell m}|^2. \tag{5}$$

Alternatively one can get the error as the diagonal of the covariance matrix of $\hat{C}_\ell^{\kappa q}$. To estimate the latter, we use 300 CMB lensing simulations and follow the steps described in § 3.2 to calculate their cross-power spectra with our BOSS quasar sample and selected quasars with DLAs. The 300 simulations of CMB lensing convergence field we adopt are part of the *Planck* 2018 release, based on MV estimate from temperature and polarization of all 300 *Planck* Full Focal Plane (FFP10) simulations (Planck Collaboration et al. 2018b) [5].

The covariance matrix element between the i-th and the j-th bin, $\mathcal{C}_{ij}$, can be estimated by

$$\mathcal{C}_{ij} = \frac{1}{N-1} \sum_{n=1}^{N} (C_{i,n} - \bar{C}_i)(C_{j,n} - \bar{C}_j) \tag{6}$$

where $N = 300$ is the total number of CMB lensing simulations, and $C_{i,n}$ denotes the i-th bin of the cross-power spectrum between the n-th mock CMB lensing simulations and our quasar sample. The error of each bin can be

---

[3] https://github.com/healpy/healpy

[4] We perform the same analysis described in this paper for different ℓ_{max} and number of bins. For BOSS QSOs, the spectrum within 10 bins with $\ell_{\mathrm{max}} = 1200$ yields the minimum χ^2. Due to the low SNR of our DLA signal, we can only give a rough estimate for the upper limit of DLA halo mass and thus we simply choose the same ℓ range and number of bins for QSOs with DLAs.

[5] The Full Focal Plane simulations are used to generate multiple mission realizations, and these maps incorporate the dominant instrumental, scanning, and data analysis effects (Planck Collaboration et al. 2016).

obtained from the square root of the variance, i.e. the diagonal of the covariance matrix:

$$\sigma_i = \sqrt{\mathcal{C}_{ii}}. \tag{7}$$

With the covariance matrix, it is convenient to compute the correlation matrix, which describes the linear correlation between pairs of bins:

$$r_{ij} = \frac{\mathcal{C}_{ij}}{\sqrt{\mathcal{C}_{ii}\mathcal{C}_{jj}}}, \tag{8}$$

with $-1 \leq r_{ij} \leq 1$. Two bins are tightly positively correlated when r is close to 1, negatively correlated when r is close to -1, and linearly uncorrelated when $r = 0$. We show the correlation matrices of lensing×quasar and lensing×DLA in Fig.3. As one can see, the off-diagonal blocks can be negligible in this case. First of all, the bins are fairly wide, and so the bin-bin covariance should be pretty small. Then, due to the big difference in the number count of the two catalogs, the overlapping part of the two catalogs is so small that their covariance can be ignored.

We adopt Eq.7 in the bias measurement, and Eq.3 in the null test (§ 5).
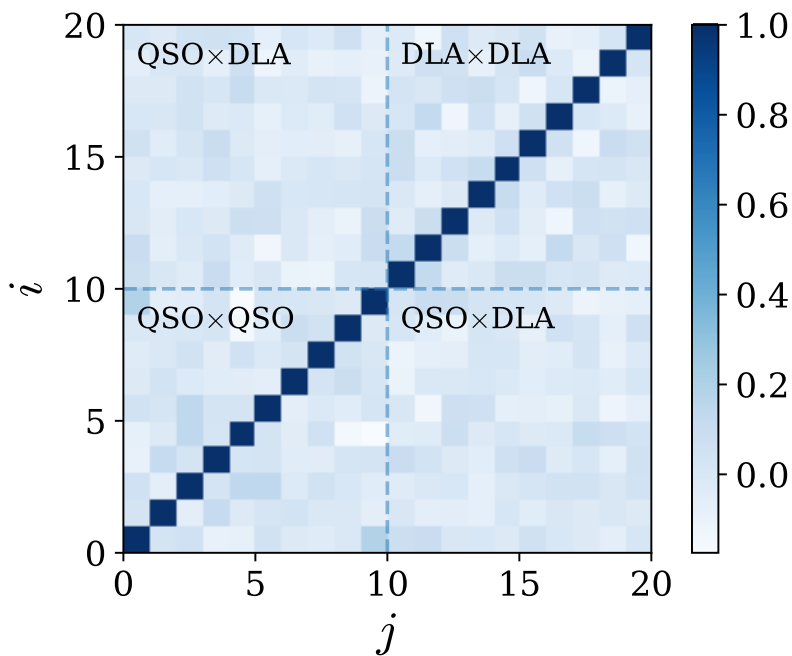
Figure 3. The correlation matrix for the BOSS QSOs and QSOs with DLAs. Here $i = 1 - 10$ denote bins in the spectrum of the BOSS QSOs and $i = 11 - 20$ denote those of QSOs with DLAs.

3.4. Analytical Model
3.4.1. Measurement of quasar bias and DLA bias

The CMB lensing convergence is defined as a weighted projection of the matter overdensity in the direction along the line of sight $\hat{n}$ (Lewis & Challinor 2006):

$$\kappa(\hat{n}) = \int_0^{z_{\rm CMB}} dz W(z)\delta_m\left(\chi(z)\hat{n}, z\right) \tag{9}$$

$\delta_m(\chi(z)\hat{n}, z)$ is the matter overdensity at redshift z in the direction $\hat{n}$, $W(z)$ is the CMB lensing kernel:

$$W(z) = \frac{3H_0^2\Omega_{m,0}}{2cH(z)}(1+z)\chi(z)\left(1 - \frac{\chi(z)}{\chi_{\rm CMB}}\right) \tag{10}$$

where H_0 is the current Hubble parameter, $H(z)$ is the Hubble parameter at redshift z, $\Omega_{m,0}$ is the current matter density, c is the speed of light, $\chi(z)$ is the comoving distance to redshift z and χ_{CMB} is the comoving distance to the last scattering surface at redshift $z_{\text{CMB}} \approx 1100$.

To relate the quasar overdensity field to the matter overdensity field, the projected surface density of quasars is given by (Peiris & Spergel 2000):

$$q(\hat{n}) = \int_0^{z_{\text{CMB}}} dz f(z) \delta_m(\chi(z)\hat{n}, z) \tag{11}$$

where $f(z)$ is its window function:

$$f(z) = \frac{b(z)dN/dz}{\left(\int dz' \frac{dN}{dz'}\right)} + \frac{3}{2H(z)}\Omega_0 H_0^2 (1+z)g(z)(5s-2) \tag{12.1}$$

$$g(z) = \frac{\chi(z)}{c} \int_z^{z_{CMB}} dz' \left(1 - \frac{\chi(z)}{\chi(z')}\right) \frac{dN}{dz'} \tag{12.2}$$

The first term is the normalized, bias-weighted redshift distribution of the quasars; the second term is the magnification bias induced by the change in the density of sources due to lensing magnification, where $s \equiv d\log_{10} N/dm$ is the response of the number density to magnification bias. Due to the multiple selection criteria, we cannot simply histogram the sample to determine s. Instead, following Krolewski et al. (2019), we get $s \approx 0.078$ for the BOSS subset and $s \approx 0.26$ for the quasars with DLAs, and just neglect the uncertainty induced by the magnification bias.

For quasars with DLAs, DLAs contribute to the cross-correlation between CMB lensing map and the quasar overdensity. Simply assuming the weak lensing signal of CMB photons is the summation of the quasar and its foreground DLA contribution, the window function in Eq.12 should be written as :

$$f(z) = \frac{\bar{n}_{\text{DLA}} b_{\text{DLA}} \cdot dN_{\text{DLA}}/dz}{\left(\int dz' \frac{dN_{\text{DLA}}}{dz'}\right)} + \frac{b_{\text{QSO}} \cdot dN_{\text{QSO}}/dz}{\left(\int dz' \frac{dN_{\text{QSO}}}{dz'}\right)} + \frac{3}{2H(z)}\Omega_0 H_0^2 (1+z)g(z)(5s-2) \tag{13}$$

$\bar{n}_{\text{DLA}}$ is the effective number count of DLAs for a single sightline. In this case it should be $N_{\text{DLA}}/N_{\text{QSO}} \approx 1.17$. Note that here N_{QSO} denotes the number of background quasars which have DLAs found in their spectra, different from N in Eq.12 referring to the number of the full quasar sample.

In a flat universe and under the Limber approximation (Limber 1953), the quasar-CMB lensing convergence angular cross-power spectrum is given by (Lewis & Challinor 2006; Sherwin et al. 2012):

$$C_\ell^{\kappa q} = \int \frac{dz}{c} \frac{H(z)}{\chi^2(z)} W(z)f(z) P_{mm}\left(k = \frac{\ell}{\chi(z)}, z\right) \tag{14}$$

where and $P_{mm}(k,z)$ is the 3D matter power spectrum.

Δz	ΔM_i	$\bar{z}$	No. of quasars	b_Q	χ^2_{red}
$2.20 \leq z \leq 2.80$	$-28.74 \leq M_i \leq -23.78$	2.434	55826	3.54 ± 0.10	1.06
$2.20 \leq z < 2.384$	$-28.70 \leq M_i \leq -23.95$	2.297	24667	3.69 ± 0.11	1.55
$2.384 \leq z < 2.643$	$-28.74 \leq M_i \leq -24.11$	2.497	24493	3.55 ± 0.15	0.61
$2.643 \leq z \leq 3.40$	$-29.31 \leq M_i \leq -24.40$	2.971	24724	3.57 ± 0.09	0.66
$2.20 \leq z \leq 2.80$	$-28.74 \leq M_i < -26.19$	2.456	18477	3.69 ± 0.10	2.19
$2.20 \leq z \leq 2.80$	$-26.19 \leq M_i < -25.36$	2.436	18790	3.56 ± 0.13	1.71
$2.20 \leq z \leq 2.80$	$-25.36 \leq M_i \leq -23.78$	2.411	18559	3.81 ± 0.19	0.4

Table 2. Clustering results for NGC-CORE sample and subsamples in Eftekharzadeh et al. (2015) (Table 5 in their paper). The first four columns are redshift and absolute magnitude range, the average redshift and the total number of NGC quasars. Columns 5, 6 are the best-fitting bias values and the reduced χ^2 (over 7-DoF/9-DoF for the main sample/subsamples).

3.4.2. *The fiducial bias model*

We adopt the quasar bias measured in Eftekharzadeh et al. (2015) as our fiducial bias model. They report one of the most precise measurements of quasar bias for the BOSS sample using the auto-correlation approach. The quasar bias (see Table 2, repeating Table 5 in Eftekharzadeh et al. (2015)) has no significant upward trend as z increases. We use $\bar{b} = 3.60$, the average of their b_{QSO}, as the fiducial value, and assume a scaling parameter a which depicts the level of deviation from the fiducial b_{fid}:

$$b = a \cdot b_{\mathrm{fid}} \tag{15}$$

As a test, we also adopt the bias-redshift model derived in Laurent et al. (2017) to guarantee the robustness of our analysis. More details are shown in Appendix A.

3.4.3. *From bias to halo mass*

We use the fitting formula in Tinker et al. (2010) to relate the bias to the peak height of the linear density field ν (Press & Schechter 1974; Sheth et al. 2001):

$$\nu = \frac{\delta_c}{\sigma(M_\Delta)}$$
$$b(\nu) = 1 - A\frac{\nu^\alpha}{\nu^\alpha + \delta_c^\alpha} + B\nu^\beta + C\nu^\gamma \tag{16}$$

where $A = 1.0 + 0.24y\exp\left[-(4/y)^4\right]$, $\alpha = 0.44y - 0.88$, $B = 0.183$, $\beta = 1.5$, $C = 0.019 + 0.107y + 0.19\exp\left[-(4/y)^4\right]$ and $\gamma = 2.4$ if we assume $y = log_{10}\Delta$. $\delta_c = 1.686$ is the critical overdensity for collapse, and $\sigma(M_\Delta)$ is the linear matter variance on the Lagrangian scale of the halo.

In this work we assume $\Delta = 200$ and thus M refers to the total mass within the radius r_{200} at which the enclosed mass density is 200 times the average matter density of the Universe:

$$M_{200} = \frac{800\pi}{3}\rho_{\mathrm{m}}(z)r_{200}^3. \tag{17}$$

COLOSSUS[6] (Diemer 2018) is a convenient tool to derive M from the peak height ν. Since the relation between bias and ν is slightly complicated, we invert the mass-bias relation and find the roots using `scipy`.

4. RESULTS

In this section we present our measurements of the quasar and DLA biases. We use the quasar bias measured from the BOSS sample as a prior to help us constrain the DLA bias.

4.1. *Quasar bias*

First, we cross-correlate the BOSS quasar sample with the CMB lensing map to get the maximum-likelihood estimate of b_{QSO} using Eq.2 and Eq.14. We reweight the redshift distribution of quasars in the BOSS subset following Alonso et al. (2018), so that it matches that of the QSOs with DLAs. The reweighting is to ensure the assumption that quasars in the two catalogs have similar bias. In fact, in this case reweighting the sample makes negligible difference to the final results. We run CAMB (Lewis et al. 2000) to calculate the nonlinear matter power spectrum using HALOFIT (Smith et al. 2003; Takahashi et al. 2012) . In Fig. 4, we present the cross-correlation (black point with error bar). We use the standard deviation of the fitting result as a proxy of its uncertainty, which can be derived from the resulted covariance from the curve fitting.

With the parametrization in Eq.15, we estimate the parameter $a = 0.71 \pm 0.19$ using Eq.12. This corresponds to $b_{\mathrm{QSO}} = a \cdot b_{\mathrm{fid}} = 2.55 \pm 0.70$. Following § 3.4.3, the bias value corresponds to a characteristic halo mass of $\log(M/M_\odot h^{-1}) = 11.79^{+0.63}_{-0.40}$ at a median redshift of $z_{\mathrm{m}} \approx 2.51$.

4.2. *DLA bias*

We cross-correlate the *Planck* 2018 CMB lensing map with the 17,774 quasars which have DLAs in their sightlines. If we ignore the impact of DLAs and follow the steps introduced in § 3.4.1, we obtain $a = 1.00 \pm 0.55$, deviating from the value of b_{QSO} estimated in § 4.1. Therefore, the contribution of DLAs in sightlines of quasars is not negligible.

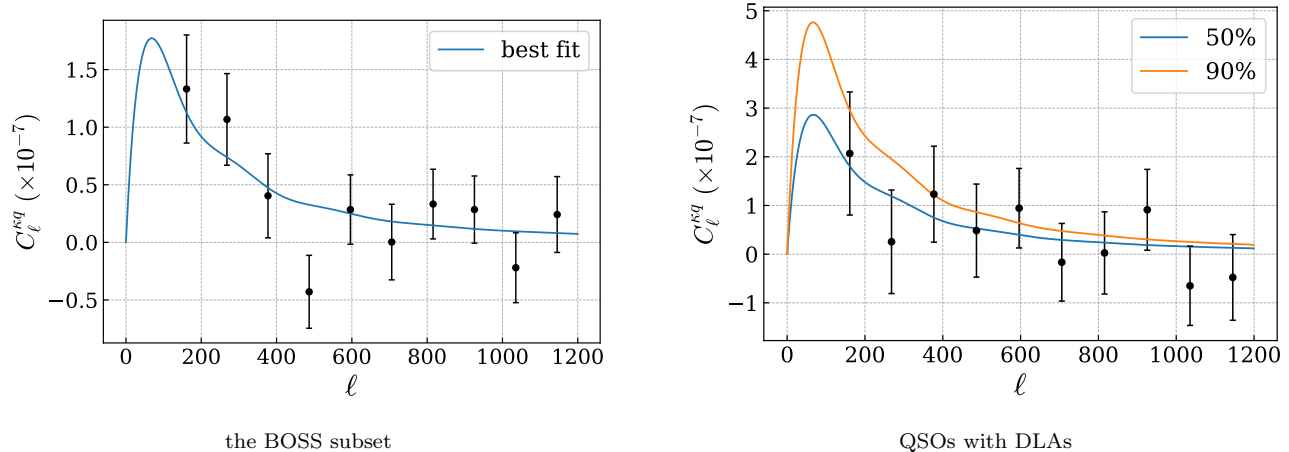
[6] https://bdiemer.bitbucket.io/colossus/

Figure 4. The CMB lensing-quasar overdensity angular cross-power spectrum for the BOSS subset (the left panel) and the QSOs with DLAs (the right panel) over the redshift range of $2.2 < z < 3.4$. In the left panel, the solid line is the best-fit theoretical curve. In the right panel, the two solid lines denote the theoretical cross-power spectra at 50% and 90% upper limits of b_{DLA}.

We measure b_{QSO} and b_{DLA} with the Markov Chain Monte Carlo (MCMC) using `emcee`[7] (Foreman-Mackey et al. 2013). Since the luminosity distribution of the BOSS subset and the selected quasars with DLAs are not significantly different (see Fig.1), we assume that b_{QSO} of quasars with DLAs approximates that of the BOSS QSO subset. Then, we assume the DLA bias b_{DLA} is a constant over the selected redshift range at $z = 2.2 - 3.4$, with a prior uniform distribution over $0 < b_{\mathrm{DLA}} < 15$ and further assume a Gaussian distribution of a as derived in § 4.1, with the central value $\mu = 0.71$ and the standard deviation $\sigma = 0.19$ as its prior distribution:

$$p(a) \sim N(\mu, \sigma^2) \tag{18}$$

The likelihood function is:

$$p(\mathbf{C}|a, b_{\mathrm{DLA}}) = \frac{1}{|\Sigma|^{\frac{1}{2}}(2\pi)^{\frac{n}{2}}} e^{-\frac{1}{2}(\hat{\mathbf{C}} - \mathbf{C})^T \Sigma^{-1}(\hat{\mathbf{C}} - \mathbf{C})} \tag{19}$$

where $\hat{C}$ is the data vector of the binned data points, $\boldsymbol{C}$ is the data vector of calculated theoretical model for the bin, and $\boldsymbol{\Sigma}$ is covariance matrix as shown in Fig.3.

We have $a = 0.68 \pm 0.18$, and $b_{\mathrm{DLA}} = 1.37^{+1.30}_{-0.92}$ corresponding to a characteristic DLA halo mass of $\log(M/M_\odot h^{-1}) = 10.60^{+1.44}_{-5.27}$ at a median redshift of $z_{\mathrm{m}} \approx 2.30$. Despite the large uncertainty, the result provides a good constraint on the upper limit of DLA halo mass, yielding $b_{\mathrm{DLA}} \leq 3.1$ and $\log(M/M_\odot h^{-1}) \leq 12.3$ at a confidence level of 90%. The results are shown in Fig.4 and Fig.5.

We have also tried to simultaneously modelling on the two catalogs, assuming that their b_{QSO} are exactly the same. The results shows that $a_{\mathrm{QSO}} = 0.67 \pm 0.19$, $b_{\mathrm{DLA}} = 1.57^{+1.33}_{-1.02}$ and the 90% upper limit of b_{DLA} is 3.30, corresponding to a halo mass of $\log(M/M_\odot h^{-1}) \leq 12.38$. This is consistent with our analysis.

5. NULL TEST

We check our result by a simple null test (Sherwin et al. 2012), calculating the cross-power spectrum between the CMB lensing convergence map on one part of the sky and the quasar map on another part of the sky. The galactic longitude of the selected part of CMB lensing map ranges from $0°$ to $100°$, and that of the 2 quasar maps ranges from $120°$ to $220°$. The error bar of the spectra is calculated by the analytical Gaussian error estimator described in § 3.3. Almost all the bins in their cross-power spectra fall within 1σ of null, as shown in Fig.6, yielding $a = 0.004 \pm 0.007$ for the BOSS subset and $a = 0.001 \pm 0.007$ for the selected quasars with DLAs.

We also correlate the 300 *Planck* FFP10 simulations with randomly-positioned quasars, and get the average of the 300 spectra as an additional null-test, yielding $a = -0.046 \pm 0.131$ for 300,000 randomly-positioned quasars within 15 bins and $a = -0.046 \pm 0.296$ for the other 100,000 quasars within 10 bins.
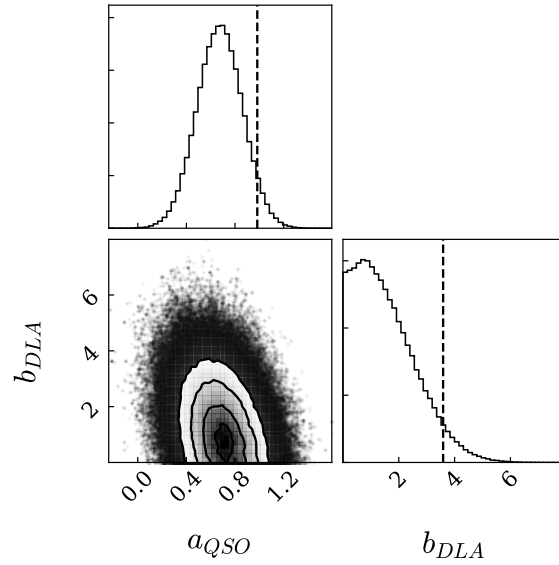
---

[7] https://github.com/dfm/emcee

Figure 5. One and two dimensional projections of the posterior probability distributions of a and b_{DLA}. The dashed lines denote the 90% upper limit, i.e. 90% of the MCMC samples in the marginalized distributions fall into its left region.
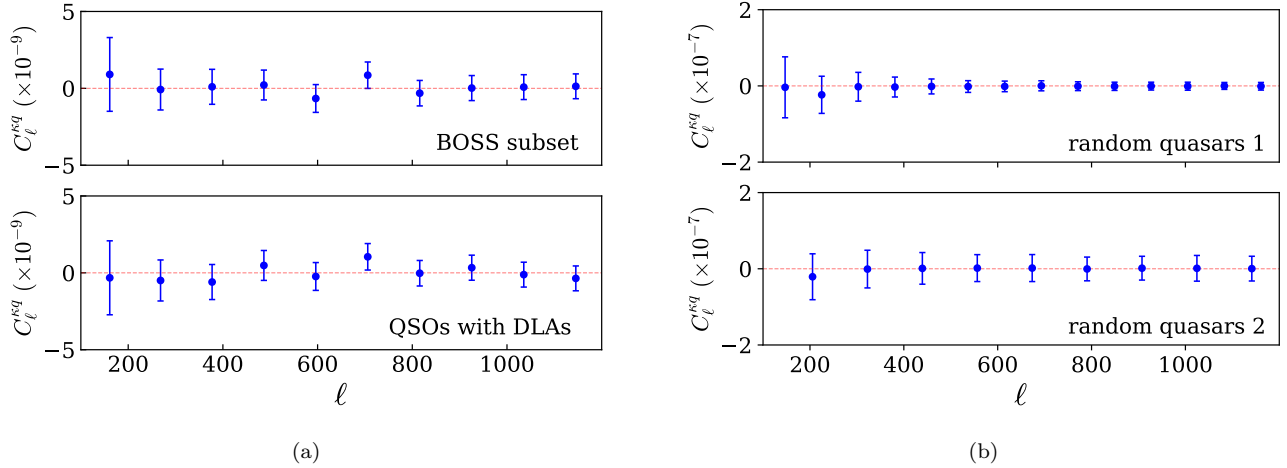

(a)   (b)

Figure 6. *Left:* Results of null tests by cross-correlating $0° \sim 100°$ of CMB lensing map and $120° \sim 220°$ of the 2 quasar maps. The error bars are obtained by Eq.3. *Right:* Results of null tests by cross-correlating the *Planck* FFP10 simulations and the 2 randomly-positioned quasar maps. Here *random quasars 1* refers to a catalog of 300,000 quasars with random positions and *random quasars 2* refers to a catalog of 100,000 quasars with random positions. The error bars are obtained by Eq.7.

6. DISCUSSION

Our measurement of bias for the BOSS subset ($a = 0.71 \pm 0.19$, $b_{\mathrm{QSO}} = 2.55 \pm 0.70$), albeit with large uncertainty, is lower than the result in Eftekharzadeh et al. (2015) measured by two-point auto-correlation function. For the DLA-CMB lensing cross-correlation, Alonso et al. (2018) pioneered using the CMB lensing convergence map to constrain the DLA bias. They used the *Planck* 2015 CMB lensing map and 2 DLA catalogs labelled as N12 (Noterdaeme et al. 2012) and G16 (Garnett et al. 2017b), both created from SDSS-III DR12. They yield constraints on the QSO bias of 2.90 ± 0.69 (2.57 ± 0.52) and DLA bias of 2.66 ± 0.93 (1.92 ± 0.69) for their N12 (G16) sample by simultaneously modelling the DLA+QSO and QSO-only measurement. Despite large uncertainties, our DLA bias has a 1.5-σ lower value than that

of Alonso et al. (2018). Comparing with Alonso et al. (2018), our study has several updates: (1) we adopt *Planck* 2018 CMB lensing convergence map and an updated DLA catalogue produced by a CNN model, currently the state-of-the-art finding algorithm for DLAs; (2) we apply similar sample selection criteria as described in Eftekharzadeh et al. (2015) so that the QSO sample we used for measuring b_{QSO} is more comparable to that of the auto-correlation results; (3) We apply the same sample selection criteria to both the BOSS quasars and the quasars with DLAs, including removing radio-loud sample, so that the measured b_{QSO} of the BOSS subset is comparable to b_{QSO} of the selected quasars with DLAs; (4) We have an updated noise calculations, quantitatively considering the different apodization size and the tSZ effects (see Appendix B). Moreover, we provide a step-by-step procedure of the cross-correlation in details for the future references.

Our results have also shown a smaller QSO bias comparing to the auto-correlation results. We have not yet found a convincing explanation for this discrepancy beyond statistical fluctuations. The systematics induced by the *Planck* and the lensing reconstruction may account for the fluctuation. Systematics related to incompleteness, random catalog generation, masking and so on may also contribute to this difference, which should be carefully considered when using the auto-correlation approach (e.g. Reid et al. 2016; Geach et al. 2019). However, the bias measurement of DLAs remains effectively immune to the unknown fluctuation of quasar bias, since b_{DLA} is subtracted from the combined lensing signal, i.e. a combination of weak lensing effect caused by both quasars and its foreground DLAs, and these quasars would share the same systematics as the selected BOSS quasars.

In this paper, we propose a meaningful upper limit for the DLA bias and our results favours a DLA halo mass of $M_{halo} < 10^{12.3} M_\odot h^{-1}$. Some observations indicate that metal-rich DLAs are hosted by massive halos with mass reaching 10^{12} $M_\odot$ (e.g., Neeleman et al. 2018), while a number of hydrodynamical simulations and astrophysical models (e.g. Pontzen et al. 2008) prefer that DLAs generally reside in smaller halos. Resolving the discrepancy in the clustering strength of DLAs is important to determine the nature of DLAs. Font-Ribera et al. (2012) measured b_{DLA} by the cross-correlation of DLA and the Lyα forest. The value of the mean bias they measured for DLAs is $b_{DLA} = 2.17 \pm 0.20$, indicating a halo mass of $\sim 10^{12} M_\odot$. Using the same technique, Pérez-Ràfols et al. (2018) updated the result using the BOSS Data Release 12. Comparing with Font-Ribera et al. (2012), Pérez-Ràfols et al. (2018) favor a lower bias, yielding $b_{DLA} = 2.00 \pm 0.19$ and corresponding to a halo mass of $\sim 4 \times 10^{11} h^{-1} M_\odot$. Using the CMB lensing with *Planck* 2018 convergence map, although the error bar of our measurement is much larger than the DLA-Lyα forest cross correlation results, our measurement provides an independent and a good constraint on the upper limit. The upper limit we pose is that the DLA halo mass is lower than $10^{12.3}$ $M_\odot h^{-1}$ at a 90% confidence level, and this is consistent with the Lyα cross-correlation measurement. The relatively low resolution (5-10 arcmin), relatively low signal-to-noise of *Planck* CMB lensing map, and the current limited sample sizes of selected quasars and DLAs may account for the large uncertainty. We expect new surveys such as DESI[8] to provide a larger quasar and DLA database, and improvements in CMB lensing, such as ACT[9], Simons Observatory (SO)[10] and CMB-S4[11], will also help a lot for a more precise bias measurement.

7. CONCLUSION

We measure the bias of DLAs by studying the cross-correlation between the selected quasars with DLAs in their sightline and CMB lensing. We perform the measurement based on the bias measured for a BOSS subset. We find a quasar bias $b_{QSO} = 2.55 \pm 0.70$ for the BOSS subset, corresponding to a quasar halo mass of $\log(M/M_\odot h^{-1}) = 11.79^{+0.63}_{-0.40}$ at a median redshift of $z_m \approx 2.51$. Our measurement of quasar bias is 2-σ smaller than the fiducial bias model (Eftekharzadeh et al. 2015). Correlated systematics between the CMB lensing map and the quasar sample might account for such a low b_{QSO}, but we have not yet found an explanation convincing enough. Despite its large uncertainty, our result provides a good constraint on the upper limit of DLAs halo mass. We find $b_{DLA} \leq 3.1$ and $\log(M/M_\odot h^{-1}) \leq 12.3$ at a confidence level of 90%, consistent with previous work (Font-Ribera et al. 2012; Pérez-Ràfols et al. 2018).

A simple null test is performed for the BOSS subset and the selected quasars with DLAs, by cross-correlating the CMB lensing convergence map on one part of the sky and the quasar map on another part of the sky. For the robustness of our measurement, we also repeat our analysis using a redshift-dependent bias model as the fiducial, and on a CMB lensing map with thermal-SZ signal deprojected (see Appendix). We expect future survey and CMB detection will improve the precision and accuracy of the DLA bias measurement..

---

[8] https://www.desi.lbl.gov/

[9] https://act.princeton.edu/

[10] https://simonsobservatory.org/

[11] https://cmb-s4.org/

APPENDIX

A. TEST FOR BIAS EVOLUTION MODEL

Adopting a model for the bias evolution with redshift is a good test for the robustness of our result. While Eftekharzadeh et al. (2015) found a roughly redshift-independent bias for the BOSS sample, other works (Shen et al. 2009; Laurent et al. 2017) found that the quasar bias sharply evolves with redshift. If the bias is redshift-dependent, the small mismatch in redshift distribution between the BOSS subset and the DLA quasars (Fig.1) could create a difference in their clustering, spuriously mimicking a change in the DLA bias. We test this possibility here by adopting an evolving bias model as an alternative to Eq.15. Laurent et al. (2017) measured the quasar correlation function of the first year of the eBOSS quasar sample, and provided a bias-redshift model by combining their results and the bias measured with the BOSS sample:

$$b_{\mathrm{QSO}}(z) = \alpha \left[(1+z)^2 - 6.565) \right] + \beta \tag{A1}$$

with $\alpha = 0.278 \pm 0.018, \beta = 2.393 \pm 0.042$. Despite the different sample selection, we adopt the central values of these parameters and use this bias model as the fiducial quasar bias in our analysis, and assume DLA bias remains a constant over the selected redshift range.

With this bias evolution model, we get $a = 0.53 \pm 0.16$, corresponding to $b_{\mathrm{QSO}} = a \cdot b_{\mathrm{fid}}(z_{\mathrm{m}}) = 2.13 \pm 0.63$ and a characteristic halo mass of $\log(M/M_\odot h^{-1}) = 11.45^{+0.48}_{-0.81}$ at a median redshift of $z_{\mathrm{m}} \approx 2.51$. Furthermore, it gives $b_{\mathrm{DLA}} = 1.76^{+1.40}_{-1.11}$. The 90% upper limit of DLA bias is 3.59, corresponding to a halo of $\log(M/M_\odot h^{-1}) = 12.50$.

This result is consistent with our previous analysis.

B. TEST FOR TSZ-FREE LENSING SIGNAL

Thermal Sunyaev-Zel'dovich (tSZ) contamination is considered to be a potential systematic to CMB lensing cross-correlation analyses (van Engelen et al. 2014; Osborne et al. 2014). The Sunyaev-Zel'dovich (SZ) effect is caused by the inverse Compton scattering of CMB photons off hot electrons in the deep potential wells of galaxy clusters. Although the tSZ signal mainly comes from low-redshift structure, and is not expected to be a large source of contamination in our high-redshift analysis, it is worth testing the robustness of our result by repeating the bias measurement with tSZ-free lensing map. The Planck Collaboration released a lensing reconstruction map on `SMICA` foreground-cleaned maps, where lensing signal is estimated from temperature (TT) only with tSZ signal deprojected.

In the absence of tSZ bias, we get $a = 0.68 \pm 0.19$, $b_{\mathrm{QSO}} = a \cdot b_{\mathrm{fid}} = 2.45 \pm 0.70$, $log(M/M_\odot h^{-1}) = 11.72^{+0.42}_{-0.68}$ for the BOSS quasars. The 90% upper limit of DLA bias is 3.78 and that of DLA halo mass is $\log(M/M_\odot h^{-1}) = 12.58$. Fig.7 shows the data and best-fit spectra.

The consistency shows that foreground contamination is subdominant. Since the tSZ-free analysis is based on temperature maps only and lacking polarization information, we take the measurement on the MV estimated lensing signal as our primary conclusion.

---

[12] https://support.cosmos.esa.int/pla/

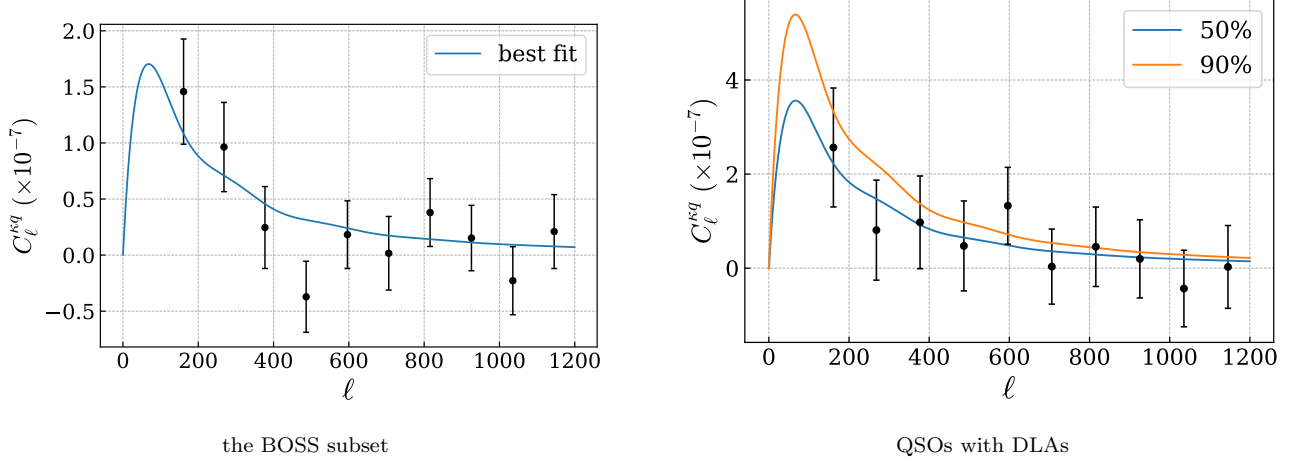[13] http://www.esa.int/Planck

[14] http://www.sdss.org

Figure 7. Cross-power spectrum on tSZ-free lensing signal with the BOSS subset (the left panel) and with the QSOs with DLAs (the right panel) over the redshift range of $2.2 < z < 3.4$. In the left panel, the solid line is the best-fit theoretical curve. In the right panel, the two solid lines denote the theoretical cross-power spectra at 50% and 90% upper limits of b_{DLA}.

C. TEST FOR ANOTHER DLA CATALOG

Ho et al. (2020) provided an revised DLA catalog using Gaussian processes. Their pipeline improved the ability to detect multiple DLAs along a single sightline. They analysed 158,825 Lyman-α spectra selected from SDSS DR12 and present updated estimates for the statistical properties of DLAs, including the column density distribution function, line density, and neutral hydrogen density. We apply our sample selection criteria to their DLA catalog as described in §2.4 except the DLA `confidence` (they don't have such a parameter in their catalog), and get 12,368 quasars with 17,836 foreground DLAs. Fig. 8 shows the properties of the selected sample. Also we repeat the steps in §3.3 to calculate the corresponding covariance matrix.

With this new DLA catalog we get $a = 0.78 \pm 0.20$, $b_{\mathrm{QSO}} = 2.79 \pm 0.72$ for the BOSS quasars. As for DLAs, we obtain $b_{\mathrm{DLA}} = 2.71^{+1.28}_{-1.25}$. This result is perfectly consistent with that in Alonso et al. (2018). The 90% upper limit of b_{DLA} is 4.34, corresponding to a halo of $\log(M/M_{\odot}h^{-1}) = 12.69$. Fig.9 shows the data and best-fit spectra.
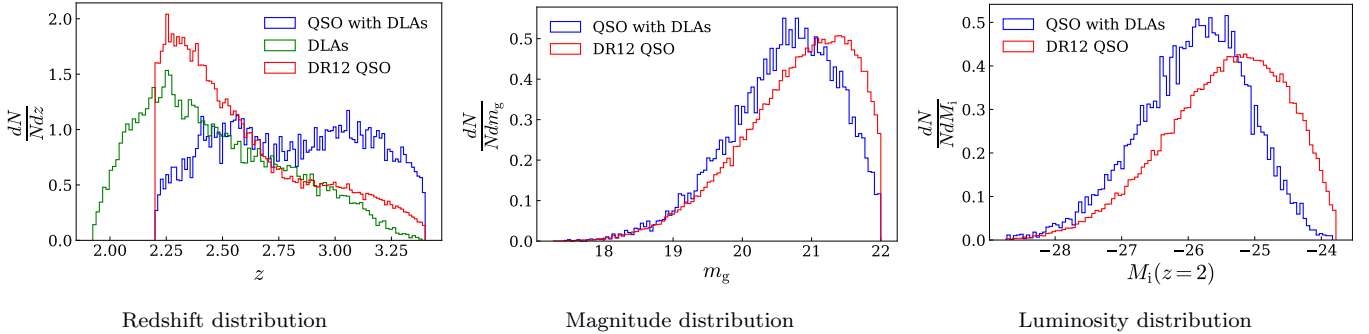
Figure 8. The normalised redshift, magnitude and luminosity distributions of the selected BOSS quasar and DLA samples in the Ho et al. (2020) catalog.

D. APODIZATION

We use mocks to to decide a proper kernel size. For each mock, we start with theoretical curves $C_{\ell}^{\kappa\kappa}$, C_{ℓ}^{qq} and $C_{\ell}^{\kappa q}$ given by:

$$
\begin{aligned}
C_{\ell}^{\kappa\kappa} &= \int \frac{dz}{c} \frac{H(z)}{\chi^2(z)} W^2(z) P_{mm}(k = \tfrac{\ell}{\chi(z)}, z), \\
C_{\ell}^{qq} &= \int \frac{dz}{c} \frac{H(z)}{\chi^2(z)} f^2(z) P_{mm}(k = \tfrac{\ell}{\chi(z)}, z), \\
C_{\ell}^{\kappa q} &= \int \frac{dz}{c} \frac{H(z)}{\chi^2(z)} W(z) f(z) P_{mm}(k = \tfrac{\ell}{\chi(z)}, z).
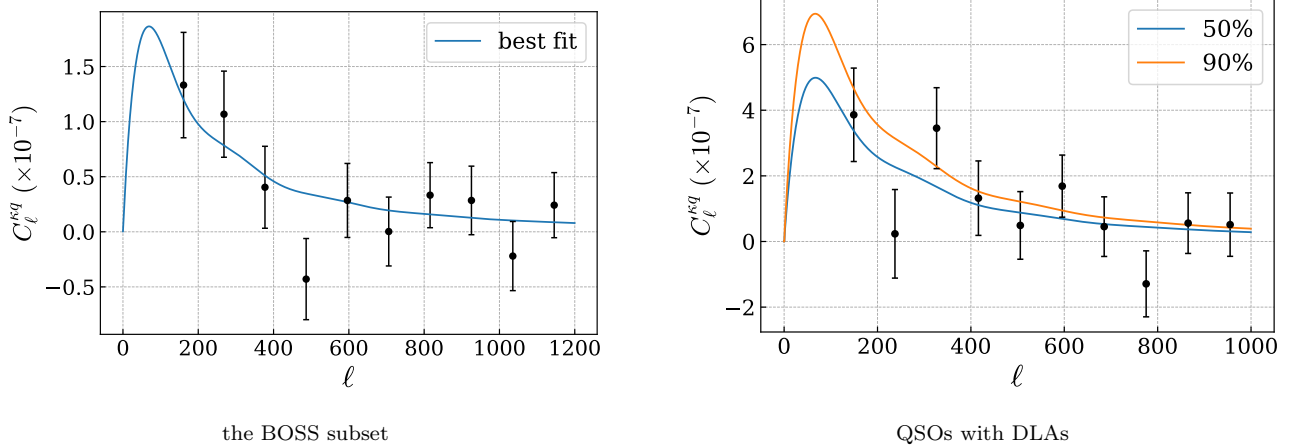\end{aligned}
\tag{D2}
$$

Figure 9. Cross-power spectrum on CMB lensing signal with the BOSS subset (the left panel) and with the QSOs with DLAs in the Ho et al. (2020) catalog (the right panel) over the redshift range of $2.2 < z < 3.4$. In the left panel, the solid line is the best-fit theoretical curve. In the right panel, the two solid lines denote the theoretical cross-power spectra at 50% and 90% upper limits of b_{DLA}.

See more details of these equations in §3.4. We draw a sample of 2×10^8 quasars with the bias $b_{\mathrm{QSO}} = 2.5$ uniformly distributed over the redshift range of $2.2 \leq z \leq 3.4$. We then generate Gaussian-distributed correlated CMB lensing and quasar fields through `healpy.synfast` following Eq.13 and Eq.14 in Serra et al. (2014):

$$
\begin{aligned}
a_{\ell m}^{\kappa\kappa} &= \xi_a \left(C_\ell^{\kappa\kappa}\right)^{1/2} \\
a_{\ell m}^{qq} &= \xi_a C_\ell^{\kappa q} / \left(C_\ell^{\kappa\kappa}\right)^{1/2} + \xi_b \left(C_\ell^{qq} - \left(C_\ell^{\kappa q}\right)^2 / C_\ell^{\kappa\kappa}\right)^{1/2}
\end{aligned}
\tag{D3}
$$

where ξ denotes a random amplitude so that $\langle \xi \xi^* \rangle = 1$ and $\langle \xi \rangle = 0$, yielding

$$
\begin{aligned}
\langle a_{\ell m}^{\kappa\kappa} a_{\ell m}^{\kappa\kappa*} \rangle &= C_\ell^{\kappa\kappa}, \\
\langle a_{\ell m}^{\kappa\kappa} a_{\ell m}^{qq*} \rangle &= C_\ell^{\kappa q}, \\
\langle a_{\ell m}^{qq} a_{\ell m}^{qq*} \rangle &= C_\ell^{qq}.
\end{aligned}
\tag{D4}
$$

We multiply the synthetic Gaussian maps by the original binary masks, to ensure that pixels without data remain empty, such as regions around the Galactic plane. We then apply the apodized mocks with FWHM given in Table 1 before measurement of cross-power spectra. We repeat these steps on 200 Gaussian mocks, average them together and bin them into 10 bands. By comparing the binned average reconstructed spectra $\hat{C}_i^{\kappa q}$ and the binned theoretical template $C_i^{\kappa q}$ and calculating the mean squared error (MSE) of the residuals:

$$
\mathrm{MSE} = \sum_{i=1}^{N} \frac{(\hat{C}_i^{\kappa q} - C_i^{\kappa q})^2}{N}
\tag{D5}
$$

where $N = 10$.

<div align="center">REFERENCES</div>

Alonso, D., Colosimo, J., Font-Ribera, A., & Slosar, A. 2018, JCAP, 2018, 053, doi: 10.1088/1475-7516/2018/04/053

Becker, R. H., White, R. L., & Helfand, D. J. 1995, ApJ, 450, 559, doi: 10.1086/176166

Berry, M., Somerville, R. S., Gawiser, E., et al. 2016, MNRAS, 458, 531, doi: 10.1093/mnras/stw231

Bianchini, F., Bielewicz, P., Lapi, A., et al. 2015, ApJ, 802, 64, doi: 10.1088/0004-637X/802/1/64

Busca, N. G., Delubac, T., Rich, J., et al. 2013, A&A, 552, A96, doi: 10.1051/0004-6361/201220724

Cabré, A., Fosalba, P., Gaztañaga, E., & Manera, M. 2007, Monthly Notices of the Royal Astronomical Society, 381, 1347, doi: 10.1111/j.1365-2966.2007.12280.x

Cai, Z., Fan, X., Noterdaeme, P., et al. 2014, The Astrophysical Journal, 793, 139, doi: 10.1088/0004-637x/793/2/139

Carron, J., & Lewis, A. 2017, PhRvD, 96, 063510, doi: 10.1103/PhysRevD.96.063510

Chen, H.-W., Kennicutt, Robert C., J., & Rauch, M. 2005, ApJ, 620, 703, doi: 10.1086/427088

Cooke, J., Wolfe, A. M., Gawiser, E., & Prochaska, J. X. 2006, ApJL, 636, L9, doi: 10.1086/499779

Dawson, K. S., Schlegel, D. J., Ahn, C. P., et al. 2013, AJ, 145, 10, doi: 10.1088/0004-6256/145/1/10

Diemer, B. 2018, ApJS, 239, 35, doi: 10.3847/1538-4365/aaee8c

Donoso, E., Li, C., Kauffmann, G., Best, P. N., & Heckman, T. M. 2010, MNRAS, 407, 1078, doi: 10.1111/j.1365-2966.2010.16907.x

Efstathiou, G. 2004, MNRAS, 349, 603, doi: 10.1111/j.1365-2966.2004.07530.x

Eftekharzadeh, S., Myers, A. D., White, M., et al. 2015, MNRAS, 453, 2779, doi: 10.1093/mnras/stv1763

Eisenstein, D. J., Weinberg, D. H., Agol, E., et al. 2011, AJ, 142, 72, doi: 10.1088/0004-6256/142/3/72

Ferraro, S., Hill, J. C., Battaglia, N., Liu, J., & Spergel, D. N. 2016, PhRvD, 94, 123526, doi: 10.1103/PhysRevD.94.123526

Font-Ribera, A., Miralda-Escudé, J., Arnau, E., et al. 2012, JCAP, 2012, 059, doi: 10.1088/1475-7516/2012/11/059

Foreman-Mackey, D., Hogg, D. W., Lang, D., & Goodman, J. 2013, PASP, 125, 306, doi: 10.1086/670067

Fumagalli, M., O'Meara, J. M., Prochaska, J. X., Rafelski, M., & Kanekar, N. 2015, MNRAS, 446, 3178, doi: 10.1093/mnras/stu2325

Fynbo, J. P. U., Laursen, P., Ledoux, C., et al. 2010, MNRAS, 408, 2128, doi: 10.1111/j.1365-2966.2010.17294.x

Garnett, R., Ho, S., Bird, S., & Schneider, J. 2017a, MNRAS, 472, 1850, doi: 10.1093/mnras/stx1958

—. 2017b, MNRAS, 472, 1850, doi: 10.1093/mnras/stx1958

Geach, J. E., Peacock, J. A., Myers, A. D., et al. 2019, ApJ, 874, 85, doi: 10.3847/1538-4357/ab0894

Giannantonio, T., Fosalba, P., Cawthon, R., et al. 2016, MNRAS, 456, 3213, doi: 10.1093/mnras/stv2678

Górski, K. M., Hivon, E., Banday, A. J., et al. 2005, ApJ, 622, 759, doi: 10.1086/427976

Han, J., Ferraro, S., Giusarma, E., & Ho, S. 2019, MNRAS, 485, 1720, doi: 10.1093/mnras/stz528

Hennawi, J. F., Prochaska, J. X., Kollmeier, J., & Zheng, Z. 2009, ApJL, 693, L49, doi: 10.1088/0004-637X/693/2/L49

Hivon, E., Górski, K. M., Netterfield, C. B., et al. 2002, ApJ, 567, 2, doi: 10.1086/338126

Ho, M.-F., Bird, S., & Garnett, R. 2020, MNRAS, 496, 5436, doi: 10.1093/mnras/staa1806

Johnson-Groh, M., Marois, C., & Ellison, S. L. 2016, ApJ, 831, 49, doi: 10.3847/0004-637X/831/1/49

Jones, E., Oliphant, T., & Peterson, P. 2001

Krogager, J. K., Møller, P., Fynbo, J. P. U., & Noterdaeme, P. 2017, MNRAS, 469, 2959, doi: 10.1093/mnras/stx1011

Krolewski, A., Ferraro, S., Schlafly, E. F., & White, M. 2019, arXiv e-prints, arXiv:1909.07412. https://arxiv.org/abs/1909.07412

Kulkarni, V., York, D. G., Vladilo, G., & Welty, D. E. 2006, Infrared Observations of Dusty Quasar Absorption Systems: Dust Composition and Absorber Environment, Spitzer Proposal

Laurent, P., Eftekharzadeh, S., Le Goff, J.-M., et al. 2017, JCAP, 2017, 017, doi: 10.1088/1475-7516/2017/07/017

Le Brun, V., Bergeron, J., Boisse, P., & Deharveng, J. M. 1997, A&A, 321, 733. https://arxiv.org/abs/astro-ph/9611031

Lee, T. S., Nagamine, K., Hernquist, L., & Springel, V. 2011, MNRAS, 411, 54, doi: 10.1111/j.1365-2966.2010.17668.x

Lewis, A., & Challinor, A. 2006, PhR, 429, 1, doi: 10.1016/j.physrep.2006.03.002

Lewis, A., Challinor, A., & Lasenby, A. 2000, ApJ, 538, 473, doi: 10.1086/309179

Limber, D. N. 1953, ApJ, 117, 134, doi: 10.1086/145672

Møller, P., Fynbo, J. P. U., Ledoux, C., & Nilsson, K. K. 2013, MNRAS, 430, 2680, doi: 10.1093/mnras/stt067

Møller, P., Warren, S. J., Fall, S. M., Fynbo, J. U., & Jakobsen, P. 2002, ApJ, 574, 51, doi: 10.1086/340934

Nagamine, K., Springel, V., & Hernquist, L. 2004, Monthly Notices of the Royal Astronomical Society, 348, 421, doi: 10.1111/j.1365-2966.2004.07393.x

Neeleman, M., Kanekar, N., Prochaska, J. X., et al. 2018, ApJL, 856, L12, doi: 10.3847/2041-8213/aab5b1

Neeleman, M., Prochaska, J. X., Kanekar, N., & Rafelski, M. 2020, Nature, 581, 269, doi: 10.1038/s41586-020-2276-y

Noterdaeme, P., Petitjean, P., Carithers, W. C., et al. 2012, A&A, 547, L1, doi: 10.1051/0004-6361/201220259

Osborne, S. J., Hanson, D., & Doré, O. 2014, JCAP, 2014, 024, doi: 10.1088/1475-7516/2014/03/024

Ota, K., Walter, F., Ohta, K., et al. 2014, ApJ, 792, 34, doi: 10.1088/0004-637X/792/1/34

Pâris, I., Petitjean, P., Ross, N. P., et al. 2017, A&A, 597, A79, doi: 10.1051/0004-6361/201527999

Parks, D., Prochaska, J. X., Dong, S., & Cai, Z. 2018, MNRAS, 476, 1151, doi: 10.1093/mnras/sty196

Peiris, H. V., & Spergel, D. N. 2000, The Astrophysical Journal, 540, 605, doi: 10.1086/309373

Pérez-Ràfols, I., Font-Ribera, A., Miralda-Escudé, J., et al. 2018, MNRAS, 473, 3019, doi: 10.1093/mnras/stx2525

Planck Collaboration, Ade, P. A. R., Aghanim, N., et al. 2016, A&A, 594, A12, doi: 10.1051/0004-6361/201527103

Planck Collaboration, Aghanim, N., Akrami, Y., et al. 2018a, arXiv e-prints, arXiv:1807.06209. https://arxiv.org/abs/1807.06209

—. 2018b, arXiv e-prints, arXiv:1807.06210. https://arxiv.org/abs/1807.06210

Pontzen, A., Governato, F., Pettini, M., et al. 2008, MNRAS, 390, 1349, doi: 10.1111/j.1365-2966.2008.13782.x

Press, W. H., & Schechter, P. 1974, ApJ, 187, 425, doi: 10.1086/152650

Pullen, A. R., Alam, S., He, S., & Ho, S. 2016, MNRAS, 460, 4098, doi: 10.1093/mnras/stw1249

Reid, B., Ho, S., Padmanabhan, N., et al. 2016, Monthly Notices of the Royal Astronomical Society, 455, 1553, doi: 10.1093/mnras/stv2382

Retana-Montenegro, E., & Röttgering, H. J. A. 2017, A&A, 600, A97, doi: 10.1051/0004-6361/201526433

Richards, G. T., Strauss, M. A., Fan, X., et al. 2006, AJ, 131, 2766, doi: 10.1086/503559

Rudie, G. C., Newman, A. B., & Murphy, M. T. 2017, ApJ, 843, 98, doi: 10.3847/1538-4357/aa74d7

Serra, P., Lagache, G., Doré, O., Pullen, A., & White, M. 2014, A&A, 570, A98, doi: 10.1051/0004-6361/201423958

Shen, Y., Strauss, M. A., Ross, N. P., et al. 2009, ApJ, 697, 1656, doi: 10.1088/0004-637X/697/2/1656

Sherwin, B. D., Das, S., Hajian, A., et al. 2012, PhRvD, 86, 083006, doi: 10.1103/PhysRevD.86.083006

Sheth, R. K., Mo, H. J., & Tormen, G. 2001, MNRAS, 323, 1, doi: 10.1046/j.1365-8711.2001.04006.x

Smith, R. E., Peacock, J. A., Jenkins, A., et al. 2003, MNRAS, 341, 1311, doi: 10.1046/j.1365-8711.2003.06503.x

Takahashi, R., Sato, M., Nishimichi, T., Taruya, A., & Oguri, M. 2012, ApJ, 761, 152, doi: 10.1088/0004-637X/761/2/152

Tinker, J. L., Robertson, B. E., Kravtsov, A. V., et al. 2010, ApJ, 724, 878, doi: 10.1088/0004-637X/724/2/878

van Engelen, A., Bhattacharya, S., Sehgal, N., et al. 2014, ApJ, 786, 13, doi: 10.1088/0004-637X/786/1/13

Vielva, P., & Sanz, J. L. 2010, Monthly Notices of the Royal Astronomical Society, 404, 895, doi: 10.1111/j.1365-2966.2010.16318.x

Wandelt, B. D., Hivon, E., & Górski, K. M. 2001a, PhRvD, 64, 083003, doi: 10.1103/PhysRevD.64.083003

—. 2001b, PhRvD, 64, 083003, doi: 10.1103/PhysRevD.64.083003

White, M., Myers, A. D., Ross, N. P., et al. 2012, MNRAS, 424, 933, doi: 10.1111/j.1365-2966.2012.21251.x

Wolfe, A. M., Gawiser, E., & Prochaska, J. X. 2005, ARA&A, 43, 861, doi: 10.1146/annurev.astro.42.053102.133950

Wolfe, A. M., Turnshek, D. A., Smith, H. E., & Cohen, R. D. 1986, ApJS, 61, 249, doi: 10.1086/191114

Zafar, T., Møller, P., Ledoux, C., et al. 2011, A&A, 532, A51, doi: 10.1051/0004-6361/201016332